# A 33.7% Tx Efficiency Crystal-Less BLE-Compatible Transmitter with Adaptive PA Output Power Calibration for Ingestible Devices

Saebyeok Shin, Jaehong Jung, Giovanni Traverso, and Anantha P. Chandrakasan
*Massachusetts Institute of Technology*, Cambridge, MA, USA
saebyeok@mit.edu

***Abstract*—This paper presents a Bluetooth Low Energy (BLE)-compatible transmitter (Tx) for the ingestible devices. To compensate for the varying communication losses caused by the surrounding environment, we propose the PA output power ($P_{PA}$) calibration scheme, adaptively adjusting the supply voltage of the class-D power amplifier (DPA) through the dedicated LDO with the output power tuning range of 11.6 dB. This calibration is performed within the BLE preamble interval without sacrificing the additional latency. Moreover, the dual-mode operations of DPA configuring P-over-N PA and N-over-N PA maximize the PA efficiency of 49.7 % and 54 % at 1.6 dBm and -10 dBm, respectively. Also, the proposed 2.4 GHz Tx supports GFSK modulation while meeting the BLE requirements without external crystal. Through wireless evaluation, the proposed BLE-compatible Tx maintains a constant input power of the receiver (Rx) ($P_{RX}$) under diverse conditions, thus alleviating the Rx sensitivity requirement and PVT variation of DPA.**

***Index Terms*—biomedical system, ingestible device, low-power radio, system-on-chip, BLE, Class-D power amplifier**

## I. Introduction

Ingestible devices [1] are promising sensors to obtain various healthcare indication data. A Tx operation should be robust to various surrounding environments for successful wireless communication from within the gastric fluid to the outside of the body. Based on the link budget analysis (Fig. 1) incorporating the signal loss through the body [2] and the external receiver sensitivity [3], a transmitted power ($P_{OUT}$) of –10 dBm is required. However, dynamic variations—such as changes in pH, amount of fluid and its concentration—can further introduce additional path losses caused by the matching issue of the antenna. As depicted in Fig. 2 (a), a 350 ml volume increase in simulated gastric fluid (SGF) results in a 13 dB loss [4]. The measured normalized loss at different pH levels (Fig. 2 (b)) is 19 dB worse in pH 1 compared to pH 7. Moreover, in ingestible devices, using large $P_{OUT}$ to compensate for unpredictable losses is strictly prohibited due to the peak power limit for human body safety [5] and restricted battery capacity.

To overcome these issues, this paper proposes crystal-less BLE-compatible Tx with packet-frame adaptive PA output power calibration for ingestible devices compensating the loss caused by impedance mismatch. Adjusting the supply voltage of DPA ($V_{DD,PA}$) allows the system to maintain consistent $P_{RX}$ under varying conditions. This paper is organized as follows. Section II elaborates on the proposed packet-frame adaptive PA output power calibration. Section III details the circuit-level implementation of the Tx. Section IV presents and analyzes the measurement results, and Section V concludes the paper.

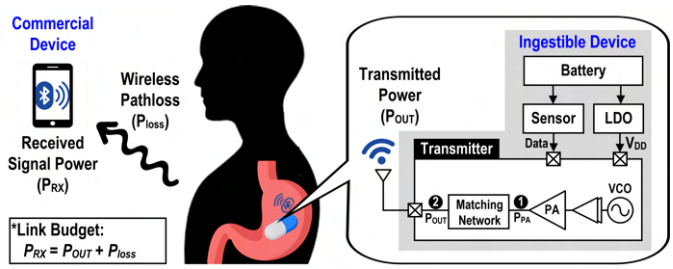


Fig. 1. Communication diagram of Tx for ingestible devices and its link budget.

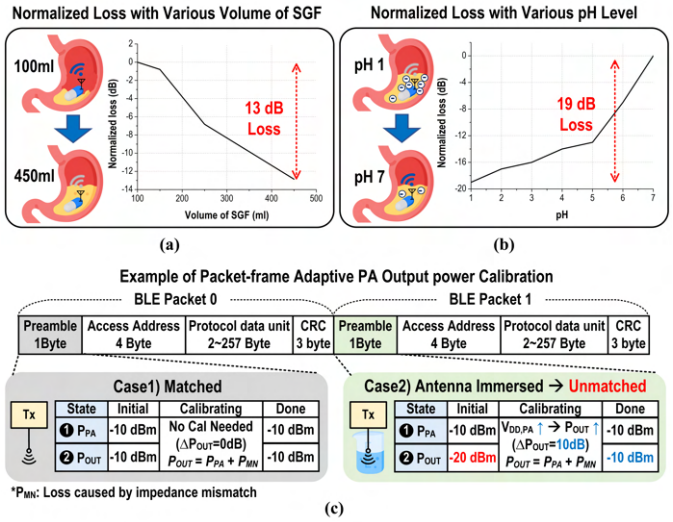


Fig. 2. (a) Additional losses of ingestible devices due to its various conditions. Normalized loss with various volume of SGF [4] and (b) measured result of normalized loss with various pH level. (c) Example of BLE packet-frame adaptive PA output power calibration.

## II. Packet-frame Adaptive PA Output Power Calibration

Fig. 2 (c) illustrates the motivation behind the proposed packet-frame adaptive PA output power calibration scheme. The on-chip impedance matching network is designed to

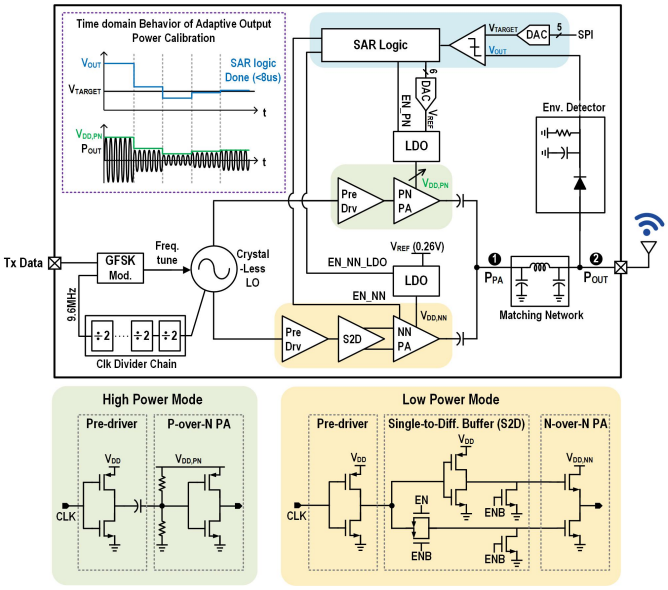


Fig. 3. System of proposed packet-frame adaptive PA output power calibration Tx and detail circuit diagram of power amplifier and pre-driver.

provide a 50 Ω match at 2.4 GHz, assuming the antenna operates in the air with a relative permittivity ($\epsilon_r$) of 1. Although this matching enables efficient power transfer in such an environment, it is optimized only for a single condition ($\epsilon_r = 1$) and thus becomes highly vulnerable to variations in the surrounding medium, common in ingestible device applications. For instance, when the antenna remains in the air (Packet 0), the impedance is well-matched, so that the output power of the DPA ($P_{\text{PA}}$) is transferred efficiently, resulting in $P_{\text{OUT}} = P_{\text{PA}}$. However, as shown in Packet 1, when the antenna is surrounded by a high-permittivity lossy medium such as gastric fluid, the matching condition deteriorates significantly. This causes increased reflection loss and a severe drop in $P_{\text{OUT}}$ falling below $-20$ dBm—around 10 dB degradation. Although the previous approach [6] has addressed these issues through matching network (MN) calibration, it incurs increased design complexity and static power overhead. Instead, the proposed design addresses the signal loss by increasing the PA output power. This approach effectively mitigates environmental variations without requiring impedance re-tuning, thereby improving communication robustness and relaxing the sensitivity requirement on the Rx. It also enhances the PVT robustness of the DPA with minimal additional circuits and power overhead.

Fig. 3 shows the schematic of the proposed system architecture, which dynamically adjusts $V_{\text{DD,PA}}$ to ensure the Tx output envelope converges to a predefined target level (-10 dBm). The envelope detector detects the amplitude of $P_{\text{OUT}}$ to compare it with the target voltage ($V_{\text{TARGET}}$) through a 1-bit comparator. The result of this comparison is fed into the SAR (Successive Approximation Register) logic and adjusts the reference voltage of LDO through the resistive digital-to-analog converter (DAC). If the amplitude of the output signal is

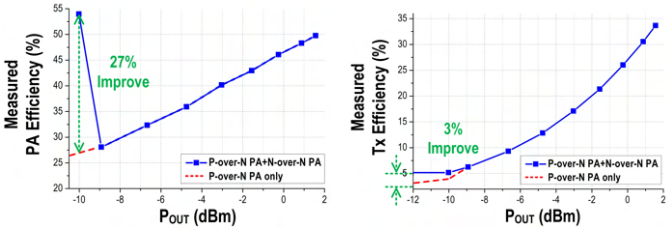


(a) (b)

Fig. 4. (a) Measured PA and (b) Tx efficiency.

below the target, the LDO output increases, effectively raising the $V_{\text{DD,PA}}$, thus boosting the output signal and vice versa. The proposed calibration loop is designed to converge within the BLE preamble interval [3], thereby avoiding any additional delay in communication.

## III. Circuit Implementation of BLE Transmitter

### A. Power-Efficient Dual-Mode Class-D Power Amplifier

To achieve the adaptive PA output power calibration, the PA should accommodate a wide $P_{\text{OUT}}$ tuning range (–10∼0 dBm). Additionally, since PA draws the majority of the power in Tx, enhancing its power efficiency across the tuning range is important. The DPA [7] is a promising solution due to its high efficiency in the low $P_{\text{OUT}}$ range. Previous work [8] segmented the output driver and controlled its number to adjust the $P_{\text{OUT}}$. However, this approach introduces off-switch parasitic components from unused drivers, resulting in unnecessary power consumption due to increased loading on the pre-driver, which further reduces efficiency at low $P_{\text{OUT}}$. In contrast, the proposed PA adjusts $V_{\text{DD,PA}}$ by employing a dedicated on-chip LDO, enabling both smaller pre-driver size and wider power tuning range while maintaining high efficiency.

Detailed circuit diagrams of DPA and pre-driver are in Fig. 3. The proposed DPA combines a high-power mode utilizing a P-over-N PA and a low-power mode employing an N-over-N PA. By controlling $V_{\text{DD,PN}}$, the $P_{\text{OUT}}$ range of P-over-N PA can be tuned from –12 to 1.6 dBm. However, at lower $P_{\text{OUT}}$ (=low $V_{\text{DD,PN}}$), the efficiency ($\eta$=$P_{\text{OUT}}$/$P_{\text{DC}}$) degrades as short-circuit current becomes the dominant contributor to PA power consumption ($P_{\text{DC}}$). To further enhance efficiency, an N-over-N PA is implemented for low-power mode, using only NMOS for both pull-up and pull-down operations. Since the NMOS gates are driven by differential clocks, the short-circuit current is effectively limited compared to P-over-N PA. As shown in Fig. 4, the high-power mode achieves a maximum $P_{\text{OUT}}$ of 1.6 dBm with an efficiency of 49.7%. In low-power mode, $P_{\text{OUT}}$ is –10 dBm with an efficiency of 54%, a 27% improvement over P-over-N PA only. Consequently, this DPA covers a wide $P_{\text{OUT}}$ range of –10 to 1.6 dBm while maintaining high PA efficiency ($> 28\%$) compared to previous work [8], [9].

### B. Auto-calibration for Optimal Power Efficiency

Fig. 5 illustrates the flow chart and timing diagram for an example converging to the low-power mode (N-over-N PA).

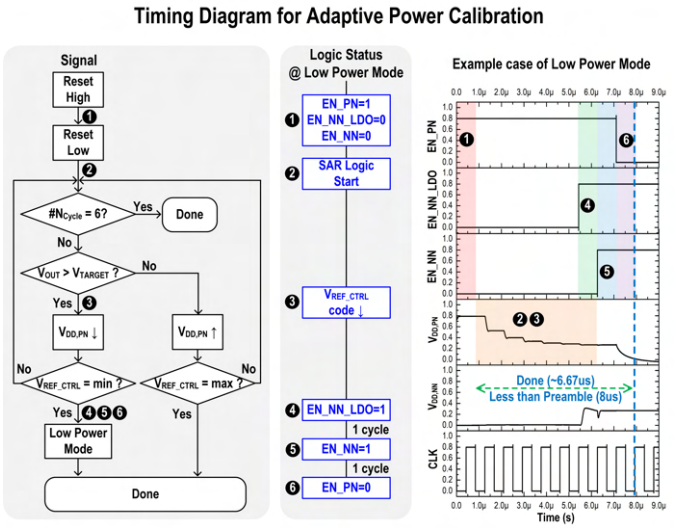


Fig. 5. Flowchart and its timing diagram for adaptive power calibration (one example converging to the low-power mode.)

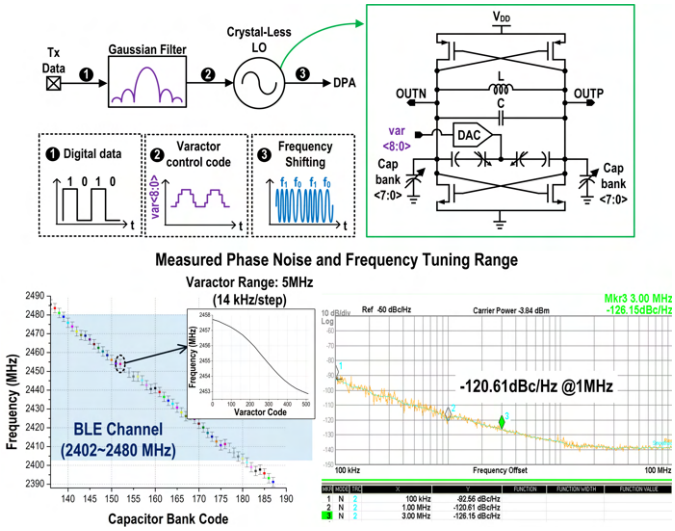


Fig. 6. Circuit diagram of BLE-compatible crystal-less LO and its measured phase noise and frequency tuning range.

The proposed dual-mode PA may cause signal discontinuity when the transition occurs from high-power mode to low-power mode. To address this issue, the P-over-N and N-over-N PAs operate concurrently during 1-cycle period, followed by transitioning fully to the low-power mode. Accordingly, this calibration ensures seamless signal during the mode transition. The SAR-based calibration time is 6.67 $\mu$s, within the preamble interval of a single BLE packet (8 $\mu$s). Consequently, Tx can deliver the data with the optimal power efficiency to the Rx; thus achieving equal $P_{\mathrm{RX}}$ on the Rx side. Once calibration is complete, the calibration logic is turned off, ensuring no additional power consumption.

### C. Crystal-Less Local Oscillator

The proposed system uses crystal-less local oscillator (LO) based on the low-power on-chip free-running LC voltage-controlled oscillator (VCO) (Fig. 6). By tuning a coarse capacitor bank, it can cover all BLE channels (2402–2480 MHz). To meet the BLE jitter requirement ($<$ 48 kHz), the varactor having 14 kHz/step is modulated by a 9-bit DAC. A one-time frequency calibration is performed during initialization. As the system operates in the stomach at a stable temperature (37°C), frequency drift remains within the jitter requirement. The on-chip Gaussian digital filter additionally processes the 9-bit DAC input signals to support the GFSK modulation. The measured phase noise at 1 MHz offset is -120 dBc/Hz, sufficiently meeting the BLE jitter requirements. Unlike the prior work employing the PLL [8], the proposed Tx eliminates the external crystal component, thus reducing the BoM cost.

## IV. Measurement Results

The proposed Tx was implemented in 65 nm CMOS, and its bench-top test setup and die micrograph are shown in Fig. 7. The GFSK modulation spectrum at a 1 Mbps data rate meets the BLE spectral mask requirements, as shown in Fig. 8.

In Fig. 9, the measured $P_{\mathrm{OUT}}$ tuning range is 11.6 dB, enabling compensation for the reflection coefficient ($|\Gamma|$) of $<$0.737 on the Smith chart, which is wider compared to the approach in [6]. Additionally, MN calibration exhibits non-uniform coverage because of the limited tuning range and nonlinear behavior of its components. By adaptively adjusting the PA output power, the proposed system overcomes the linearity limitations of conventional MNs by eliminating the nonlinear tuning components, achieving uniform and robust performance across a wide impedance space.

Wireless measurements conducted under various antenna environments (air and water) confirm that $V_{\mathrm{DD,PA}}$ can be dynamically adjusted to maintain $P_{\mathrm{RX}}$ at a similar level (Fig. 10). Table I provides detailed comparison tables with the state-of-the-art 2.4 GHz Txs. The proposed scheme achieves the best PA and Tx efficiency in both high and low $P_{\mathrm{OUT}}$ cases. Moreover, unlike previous works [7]–[9], the adaptive PA $P_{\mathrm{OUT}}$ calibration guarantees reliable BLE wireless communication in diverse biomedical environmental scenarios.

## V. Conclusion

This paper presents an on-chip fully integrated BLE Tx featuring a packet-frame adaptive PA output power calibration for ingestible devices. By dynamically adjusting the supply voltage of a dual-mode DPA based on environmental changes, the proposed system achieves consistent received

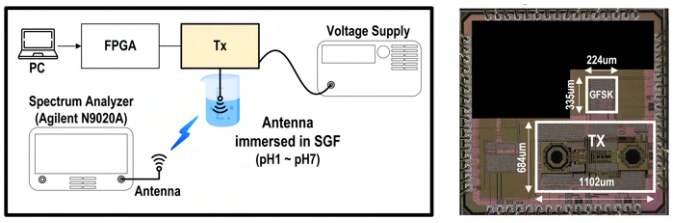


Fig. 7. Bench-top measurement setup and die micrograph

TABLE I. Comparison with state-of-the-art 2.4 GHz transmitters.

| | JSSC13 A.Paidimarri | | JSSC17 F.-W.Kuo | TCASII18 X.Peng [7] | JSSC19 S.Yang | JSSC19 X.Chen [8] | | JSSC21 M.Ding | ISSCC22 K.Shibata | RFIC24 H.Huang [9] | | This work | |
|---|---|---|---|---|---|---|---|---|---|---|---|---|---|
| Tech [nm] | 65 | | 28 | 65 | 28 | 40 | | 40 | 22 | 40 | | 65 | |
| Modulation | OOK/GMSK | | GFSK | GFSK | GFSK | GFSK | | GFSK | GFSK | 2FSK/4FSK | | GFSK | |
| $P_{OUT}$ [dBm] | High -2.5 | Low -17 | 0 | 0 | 0 | High -3.3 | Low -19.2 | 1.8 | -2 | High 0 | Low -10 | High 1.6 | Low -10 |
| $V_{DD,PA}$ [V] | 1 | 0.5 | 0.5 | 1 | 0.37 | 0.9 | 0.6 | 0.8 | 0.75 | 1.1 | 0.5 | 1[b] | 0.265 |
| $P_{TX}$ [mW] | 1.69 | 0.4 | 3.7 | 4.54 | 4 | 1.55 | 0.49 | 6.1 | 4.1 | 5.45 | 2.27 | 4.26 | 1.92 |
| PA Efficiency [%] | 40 | 17 | 32.3[a] | 40 | 30 | 39 | 10.8 | 28.2[a] | - | 28.2[a] | 27.5 | **49.7** | **54** |
| TX Efficiency [%] | 33 | 5 | 27 | 22 | 25 | 32 | 2.5 | 25 | 15.4 | 18.3 | 4.4 | **33.7** | **5.2** |
| Loss Compensation? | No | | No | No | No | No | | No | No | No | | **Yes** | |
| Area [$mm^2$] | 2 | | 1.9 | 0.5 | 0.53 | 0.0166 | | 1.05 | 0.84 | 0.48 | | 0.82 | |

[a] Calculated from power breakdown figure. [b] Adjusted by Packet-Unit Adaptive Power Control Loop.

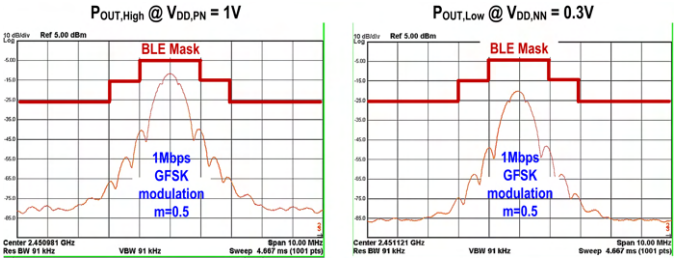


Fig. 8. Measured GFSK modulated output spectrum.

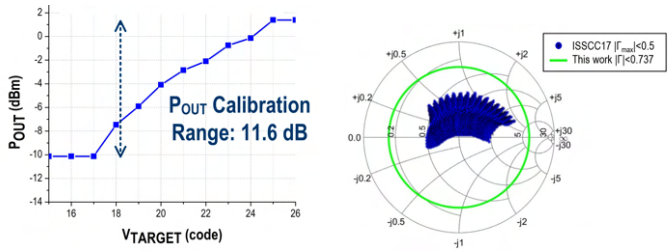


(a) (b)

Fig. 9. (a) Measured $P_{OUT}$ tuning coverage of adaptive power calibration in power domain and (b) impedance domain.

signal strength across varying gastric conditions. The calibration loop is designed to converge within the BLE preamble interval, ensuring seamless operation without communication latency overhead. Tx achieves a peak PA efficiency of 54% and a Tx efficiency of 33.7%, demonstrating state-of-the-art performance in both high and low output power modes. Further efficiency optimization across overall $P_{OUT}$ range will be possible by additionally adjusting the supply voltage of

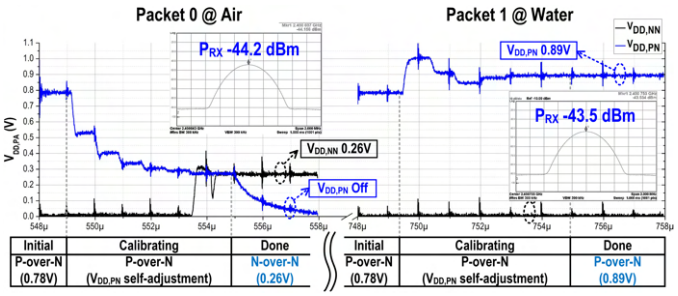


Fig. 10. Wireless measurement results with various environments (air and water).

N-over-N PA ($V_{DD,NN}$) in addition to $V_{DD,PN}$. These results validate the effectiveness of the proposed architecture for reliable low-power wireless communication in biomedical applications.

## ACKNOWLEDGMENT

This work was supported by a grant from 711 Human Performance Wing (HPW) and Defense Advanced Research Projects Agency (DARPA) under agreement number FA8650-21-2-7120. The U.S. Government is authorized to reproduce and distribute reprints for Governmental purposes notwithstanding any copyright notation thereon. The views and conclusions contained herein are those of the authors and should not be interpreted as necessarily representing the official policies or endorsements, either expressed or implied, of 711 Human Performance Wing (HPW) and Defense Advanced Research Projects Agency (DARPA) or the U.S. Government.

## REFERENCES

[1] M. Mimee, P. Nadeau, A. Hayward, S. Carim, S. Flanagan, L. Jerger, J. Collins, S. McDonnell, R. Swartwout, R. J. Citorik, V. Bulović, R. Langer, G. Traverso, A. P. Chandrakasan, and T. K. Lu, "An ingestible bacterial-electronic system to monitor gastrointestinal health," *Science*, vol. 360, no. 6391, pp. 915–918, 2018.

[2] S. Shin, Y. Jeon, I. Ballinger, M. Khan, A. Pettinari, A. Hayward, G. Traverso, and A. Chandrakasan, "A robust ble-compatible wake-up receiver for ingestible device with in-vivo evaluation," in *Proceedings of the IEEE Engineering in Medicine and Biology Conference (EMBC)*, 2024, pp. 1–5.

[3] Nordic Semiconductor, "nrf5340 product specification," 2024, https://www.nordicsemi.com/Products/Low-power-short-range-wireless/nRF5340.

[4] S. Sharma, K. B. Ramadi, N. H. Poole *et al.*, "Location-aware ingestible microdevices for wireless monitoring of gastrointestinal dynamics," *Nature Electronics*, vol. 6, pp. 242–256, 2023.

[5] *IEEE Standard for Safety Levels with Respect to Human Exposure to Electric, Magnetic and Electromagnetic Fields*, ser. IEEE Std C95.1–2019. IEEE, 2019.

[6] C. Lu, A. Ba, Y.-H. Liu, X. Wang, C. Bachmann, and K. Philips, "17.4 a sub-mw antenna-impedance detection using electrical balance for single-step on-chip tunable matching in wearable/implantable applications," in *2017 IEEE International Solid-State Circuits Conference (ISSCC)*, 2017, pp. 298–299.

[7] X. Peng, J. Yin, W.-H. Yu, P.-I. Mak, and R. P. Martins, "A coin-battery-powered ldo-free 2.4-ghz bluetooth low-energy transmitter with 34.7% peak system efficiency," *IEEE Transactions on Circuits and Systems II: Express Briefs*, vol. 65, no. 9, pp. 1174–1178, 2018.

[8] X. Chen, J. Breiholz, F. B. Yahya, C. J. Lukas, H.-S. Kim, B. H. Calhoun, and D. D. Wentzloff, "Analysis and design of an ultra-low-power bluetooth low-energy transmitter with ring oscillator-based adpll and 4 × frequency edge combiner," *IEEE Journal of Solid-State Circuits*, vol. 54, no. 5, pp. 1339–1350, 2019.

[9] H. Huang, X. Liu, Z. Tang, W. Song, Y. Ma, Y. Zhang, X. Ma, M. Zhang, J. Wang, K. Lu, Z. Wang, and G. Li, "A 0.48mm2 sub-2.4ghz transceiver with reused matching network and duty-cycle controlled class-e pa for medical band," in *2024 IEEE Radio Frequency Integrated Circuits Symposium (RFIC)*, 2024, pp. 271–274.